ELSEVIER

Thermochimica Acta 326 (1999) 105–117

thermochimica acta

Quantification of fusion in ashes from solid fuel combustion

Lone A. Hansen[a,*], Flemming J. Frandsen[a], Kim Dam-Johansen[a] Henning Sund Sørensen[b]

[a] *Department of Chemical Engineering, Technical University of Denmark, 2800, Lyngby, Denmark*
[b] *Geological Survey of Greenland and Denmark (GEUS), Thoravej 8, 2400, Copenhagen NV, Denmark*

Received 10 July 1998; accepted 29 October 1998

Abstract

The fusion of ashes produced during solid fuel combustion greatly affects the tendency of these ashes to cause operational problems in utility boilers. In this paper, a new and quantitative laboratory method for assessing the fusion of ashes based on simultaneous thermal analysis, STA, is described. Using STA, melting is detected as an endothermic reaction involving no change in mass. The measurement signals are transferred into a fusion curve showing the melt fraction in the ash as a function of temperature. This is done either by a simple comparison of the energies used for melting in different temperature ranges or by accounting for the relevant melting enthalpies. The method repeatability is good, melting onset determinations and completions generally within 10°C, and melt fractions at given temperatures generally within 10% melt. Results are presented for simple binary salt mixtures, for which the agreement with fusion as determined by phase diagrams is very good, and for straw (salt-rich) and coal (silicate-rich) ashes. Comparing ash fusion curves to index points of current standard ash fusion tests showed initial melting at temperatures typically between 50° and 100°C – but in extreme cases as low as 260°C – below the melting onset as found by the standard fusion tests. Characterizing the fusion by STA provides a more detailed description of the ash fusion as compared to conventional methods, and the onset of ash fusion is more precisely determined. Furthermore, in combination with, e.g. computer-controlled scanning electron microscopy, the method enables identification of the chemical species melting in different temperature ranges. Since ash melting has a major impact on the deposit formation tendency, the presented detailed ash fusion determination improves the prediction of problems related to ash deposition in boilers.

Keywords: Melting; Fusion; Quantification; Simultaneous thermal analysis

1. Introduction

Solid fuels used for heat and power production are composed of principally two basic classes of material: organic carbonaceous materials and inorganic species. The inorganic material is non-combustible, but for technical and economical reasons all of it cannot be removed prior to the combustion. During combustion, the inorganic species in the fuel will transform into ash which may deposit on heat-transfer surfaces in the combustion system. Accumulation of ash deposits on heat-transfer surfaces may increase the overall resistance to heat transfer, and thus lower the heat transport to the water/steam cycle leading to reduced efficiency. Uncontrolled deposit build-up on heat-transfer surfaces in a boiler can interfere with operation and cause unscheduled shut downs. With partial blockage

*Corresponding author. Tel.: +45-45-25-2859; fax: +45-45-88-2258.

0040-6031/99/$ – see front matter
PII: S0040-6031(98)00596-6

between heat-transfer tube banks, increased gas velocities may lead to increased erosion, and major incidents of internal damage due to fused material falling to the bottom of the boiler may occur. Corrosion of the heat-transfer surfaces underneath a deposit may also be increased due to ash deposits containing corrosive species. All these phenomena affect the efficiency and/or availability of a plant for power and heat generation and, consequently, the power cost. Ash deposition on heat-transfer surfaces may thus constitute a significant operational and economical problem [1,2].

The fraction of melt present in an ash particle greatly influences the ash deposition propensity in thermal fuel conversion systems. The appearance of melt is believed to increase both, the tendency for ash particles to stick to heat-transfer surfaces [1,3–5] and the subsequent rate of strength build-up in ash deposits [1,6]. For years, laboratory tests have been carried out on fuel ashes to estimate their melting behaviour, and results have been used to estimate the deposition propensity of the ashes in full-scale combustion systems.

Laboratory tests used to estimate the melting behaviour of ashes include a variety of methods. Commonly used are the conventional ash fusion tests of which many variants appear [7–10], and which is exemplified in Fig. 1 by the American standard ash fusion test, AFT. All these methods imply the controlled heat-up of an ash specimen of a well-defined shape, and the simultaneous determination of temperatures corresponding to specified geometrical shapes. In this way, the progress in melting is described by three or four characteristic temperatures (corresponding to three or four specified geometrical shapes). The main criticism of these tests has been

1. their low reproducibility;
2. unreliability in the subsequent prediction of ash behaviour in real boilers; and
3. the relevance of the laboratory prepared ash which is subjected to the test [11].

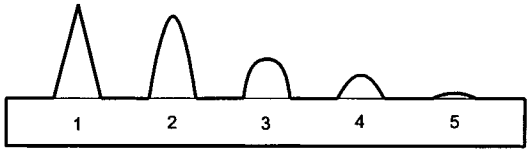

1		Cone before heating
2	IDT	Initial Deformation Temperature
3	ST	Softening Temperature (H=W)
4	HT	Hemispherical Temperature (H=½W)
5	FT	Fluid Temperature

Fig. 1. Schematic of the American Standard Ash Fusion test.

It has been emphasized that the temperature at which initial deformation is observed is not the temperature at which ash melting begins, and many coal ashes have been found to start melting at temperatures far below the initial deformation temperatures [11–14].

Alternatively, the ash-melting behaviour has been estimated based on electrical resistivity [15–18] or conductance measurements of the ash [19–21] during heat-up. These electrical quantities reflect the conduction path through the ash sample, and thereby the particle–particle contact and fusion. Both these methods detect the onset of fusion in the ash as the temperature at which the electrical properties of ash drastically changes. The electrical conductance methods have higher repeatabilities than the standard ash-fusion tests and give better predictions of field slagging performance [18]. However, these methods include some practical difficulties since satisfactory contact between ash and electrodes is hard to achieve and maintain [22]. Furthermore, the results contribute primarily with information on the onset of fusion and sintering, whereas the further melt quantity increase in the ash is harder to evaluate based on these methods.

Recently, an improved ash-fusion characterisation method based on dimensional changes of ash pellets during heating has been reported [11]. In this test, four ash cylinders are used as pillars to separate two alumina discs. As the assembly is heated, the ash pellets shrink and the distance between the tiles is measured. Significant tile movement over a narrow temperature range is interpreted to correspond to melting of distinct chemical species, and the repeatability and reproducibility of the method is reported to be high, with reproducibilities below $\pm 20^{\circ}C$ for significant tile movement (>1.5%/min).

Finally, ash melting behaviour can be estimated based on calculations. The fusion temperatures may be estimated by combining and weighing the effects of several compositional variables [23–27], or by use of chemical equilibrium calculations [28].

As indicated above, the estimation of melting behaviour of coal ashes (and the subsequent prediction of ash behaviour in real boilers) is not a simple job. The problem is further complicated, when trying to do the same job for biomass ashes. The chemical composition of biomass (i.e. in Denmark, mainly straw) is very different from that of coal and, thus, the same kind of analyses that are useful for characterizing coal ashes do not necessarily apply for biomass ashes. The standard AFT has proved to be unsuitable for ashes from biomass combustion and biomass laboratory ashes [29,30]. Thus, the present work was initiated to generate a new method to quantify the melting behaviour of biomass ashes in order to improve the understanding and prediction of ash deposition propensities during firing of biomass. In a longer term, the aim was to apply the method to coal ashes as well.

2. Experimental

2.1. Apparatus

The new method for estimating ash-melting behaviour is based on simultaneous thermal analysis (STA) and the results presented in this paper were obtained using a NETZSCH STA409. STA implies continuous measurement of sample weight (thermogravimetric analysis, TGA) and temperature differential scanning calorimetry (DSC) during heat treatment. The weight measurement reveals any mass changes taking place in the sample and by comparing the sample temperature to the temperature of an inert reference material, any heat producing or heat consuming (chemical or physical) processes occurring in the sample is detected, and the involved energy subsequently quantified.

2.2. Test method

STA was carried out on the ash samples, while heating them from 20° to typically 1390°C at 10°C/min in an N_2-atmosphere. On the resultant STA curves, melting is detected as an endothermic process involving no change in mass. Melting of a pure substance would be seen as a single endothermic peak in the DSC signal, while for 'real' ashes, the melting results in several endothermic peaks overlapping each other, corresponding to melting of the different chemical species in the ash, melting in different temperatures. Conversion of the STA curves into a melting curve is done based on a DSC signal reflecting only melting energies, which implies that energies related to other processes than melting are first subtracted from the (raw) DSC signal. Evaporation is typically occurring simultaneously to part of the melting, and evaporation enthalpies thus typically need to be quantified and subtracted. Evaporation energies are quantified as the product of a reasonably estimated evaporation enthalpy and the derivative of the TG-curve. After subtraction of evaporation enthalpies, the melting curve calculation can be carried out in one of the following two ways.

The total area below the melting curve, $A_{m,total}$, i.e. the area below the DSC curve from the first point where melting is detected, T_0 [31], and to the temperature where the melting is completed, T_{100}, reflects the total energy consumed for melting of that ash (Fig. 2). By calculating the area below the DSC curve from any temperature T_A to T_B, and dividing this area, $A_{A\text{-}B}$, by the total area below the melting curve, the fraction of 'total energy used for ash melting', which has been used in the specific temperature interval, is obtained. This energy fraction is a simple quantitative estimate of the mass fraction of ash melted in the

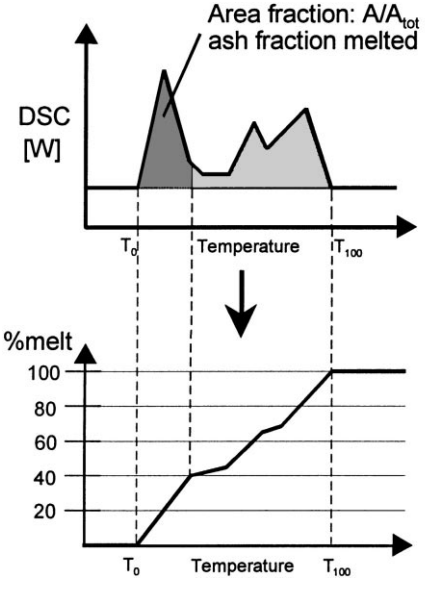

Fig. 2. Conversion of STA curve to melting curve.

specified temperature interval. This estimate is only correct, though, if the melting enthalpy of all species in the ash are alike, which is not necessarily true. The presented method thus is a simple way of determining the melting behaviour of an ash and the result expresses the melting behaviour in what could be termed an 'energy-percentage' of melt as a function of temperature.

Alternatively, a method based on quantitative determinations of the peak areas can be used: Any given peak below the melting curve corresponds to an absolute quantity of energy used for melting. The position of the peak (onset and peak temperature) gives an indication of the identity of the melting substance(s), i.e. a reasonable estimation of the relevant melting enthalpy can be made. Based on these two figures, the mass of material melted in the given temperature range can be calculated, and by relating this mass to the total mass of ash analyzed the mass fraction of ash melted in the given temperature range is obtained.

The latter method gives the most correct estimates of *mass* fraction of melted material, but this method implies that the substances melting at the different temperature intervals can be identified, so that a reasonable estimation of the involved melting enthalpies can be made (unless the species present in the ash have got equal melting enthalpies). The latter method thus implies an identification of the chemical species present in the ash (as provided, e.g. by CCSEM and XRD) and a detailed knowledge on the possible chemical reactions between the ash species.

3. Results

3.1. Simple systems

First, the melting behaviour of two simple mixtures each consisting of only two chemical species will be presented. The composition of the mixtures were chosen based on their relevance for biomass (straw) ashes and the simplicity of the corresponding phase diagrams.

3.1.1. $KCl–CaCl_2$

A sample of ≈85 mol-% KCl and 15 mol-% $CaCl_2$ was prepared and analyzed in the STA409. The resultant STA curves are shown in Fig. 3. The STA curves show evaporation (of water of crystallization from $CaCl_2 \cdot H_2O$) at 20–175°C. This is detected by (1) a decrease in mass (TG) and (2) a consumption of energy (the upward DSC peak). At 594°C, a new endothermic peak starts, with a maxima at 600°C, but also having a long 'tail' behind it, so that the peak is not quite ended until the temperature has reached 696°C. The peak corresponds to the formation of a considerable quantity of melt at the eutectic temperature, and the 'tail' corresponds to the continuous increase in melt quantity as the temperature is raised from the eutectic to the liquidus temperature. Above 700°C, the DSC-signal is greatly increased due to the evaporation of KCl (seen as the decrease in the TG curve). This experiment was repeated thrice.

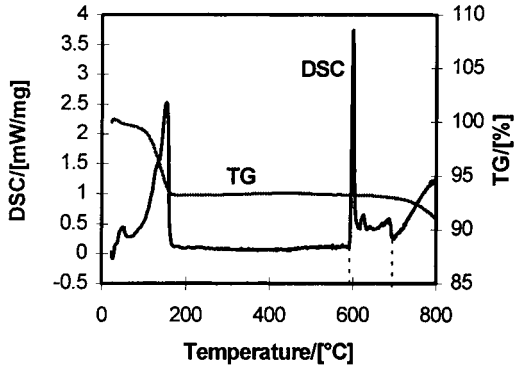

Fig. 3. STA curves for $KCl/CaCl_2$ mixture.

In Fig. 4, a comparison is made between the melting behaviour obtained by using the lever rule in the phase diagram of KCl and $CaCl_2$ [32] and the ones obtained when quantifying and comparing the areas

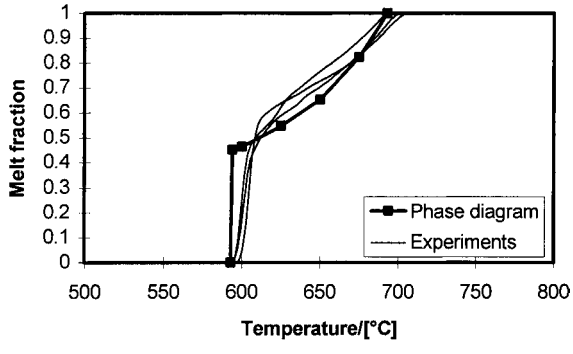

Fig. 4. Melting curves for $KCl/CaCl_2$-mixture.

Table 1
Repeatability for melting curves for KCl/$CaCl_2$-mixture

	x_{mix}/mol%	T_0/°C	Melt%(T_{eut})	T_{100}/°C	ΔH_{melt}/(J/g)
'PD' [a]	(0.85)	594	45.2	692	309.5–312.5 [b]
Exp. 1	0.853	597.1	49.4	706.7	99.7% [c]
Exp. 2	0.848	593.9	45.3	703.5	99.7% [c]
Exp. 3	0.841	593.7	49.6	695.6	99.0% [c]

[a] Found by use of phase diagram.
[b] Dependent on system composition.
[c] Fraction of theoretical melting enthalpy.

below the DSC curve for each of the three experiments. It is seen that the curve obtained from the phase diagram predicts that melting would take place instantaneously, which is not happening in reality, probably due to imperfect mixing of the salts and subsequent mass transport limitations. Except for this, though, a very good agreement between the phase-diagram-derived and the experimentally obtained melting curves is found. The deviation between the two types of curves is 10% at the maxima (neglecting the temperature range, 594–608°C, just above the eutectic temperature). Melting onset and completion deviate, respectively, <3° and 15°C from the phase diagram values. The method repeatability data is given in Table 1. Repeatability is seen to be very good, deviations are 4°C for melting onset, 4% for the melt fraction obtained at the eutectic temperature (calculated at 608°C, which is the end of the large peak), and 11°C for melting completion. Concerning the melting completion temperatures, the phase diagram shows that increasing KCl fractions increases the liquidus temperature, and this tendency is also found in the experimental results, despite the very small differences in mixture compositions. Concerning the measured melting enthalpies, a very good correlation to theoretical calculations is seen: the measured energies correspond to between 99.0 and 99.7% of the theoretical value. The theoretical and experimental description of the melting behaviour are thus judged to correlate well in this case.

3.1.2. $KCl–K_2SO_4$

The same analysis and comparison was made for a mixture of KCl and K_2SO_4, the result of which is shown in Fig. 5. As can be seen, the observed melting onset precedes the one from the phase diagram by ≈10°C, and the experimental curve overestimates the

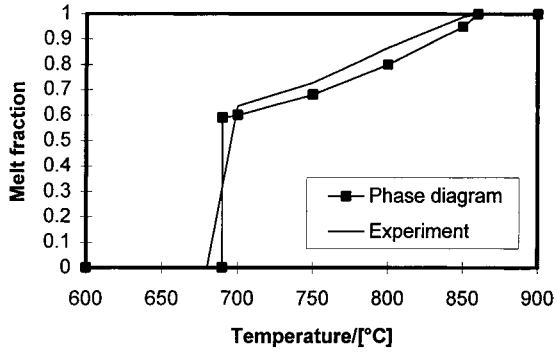

Fig. 5. Melting curves for KCl/K_2SO_4-mixture.

quantity of melt formed at the eutectic temperature with ≈4% compared to the phase-diagram-prediction. At temperatures >700°C, the deviation between experimental and the phase-diagram-derived prediction varies between four and 7%, until the curves meet at 860°C. The temperature differences between the transition temperatures given in the phase diagram and the experimentally determined ones are judged to be acceptable. This example, therefore, confirms the aforesaid and supports the assumption that STA measurements are able to describe melting behaviour of simple mixtures.

3.2. Ash samples

Several fly ash, bottom ash and deposit samples from relatively small straw-fired units have been investigated. In this paper, examples of the results will be given, representing melting behaviour results for fly ashes and bottom ashes collected during a test run of different straws at a grate-fired boiler, in addition to results for a fly ash and a bottom ash sample collected during coal combustion at a lager PF-fired

Table 2
Chemical composition of investigated ashes as oxides (%(w/w))

	SiO_2	Al_2O_3	Fe_2O_3	CaO	MgO	Na_2O	K_2O	SO_3	P_2O_5	Cl
FA1[a]	27.0	0.38	0.66	4.7	0.82	0.7	32	8.7	2.0	17
FA3 [a]	2.7	0.07	0.24	0.94	0.17	0.16	57	9.4	0.49	20
FA6 [a]	4.6	0.20	0.40	1.7	0.27	0.77	61	7.8	1.5	33
FA7 [a]	14	0.35	0.57	3.6	0.68	1.1	47	8.9	2.3	25
FA8 [a]	5.7	0.20	0.83	20	0.99	1.6	40	18	2.7	10
FA, coal [a]	55	18.2	6.4	1.6	1.5	0.5	1.9	0.4	0.2	—
BA1 [b]	68	0.9	0.56	10	2	0.4	11	0.3	1.8	0.15
BA3 [b]	46	0.84	0.34	15	2.5	1.6	24	0.29	2.6	0.19
BA6 [b]	60	0.57	0.37	11	2.2	0.35	21	0.35	2.7	0.73
BA7 [b]	63	1.7	0.65	14	2.7	1.0	17	0.27	2.6	0.30
BA8 [b]	53	1	0.51	16	2.5	0.9	20	0.31	3.1	0.20
BA, coal [b]	61	16	8.2	2.0	1.6	0.5	1.6	0.69	0.15	—

[a] Fly ash, number indicates experiment number for straw firing experiments.
[b] Bottom ash, number indicates experiment number for straw firing experiments.

boiler. More results for ashes collected during coal/straw co-firing at a PF-fired boiler are presented elsewhere [33].

The chemical compositions of the ashes investigated are given on an oxide basis in Table 2, but since not only the elemental composition but also the association of elements bears significance for determining the melting behaviour, the dominant species in the ashes, as found by computer-controlled scanning electron microscopy (CCSEM) [34,35], are presented in Table 3. The CCSEM identifies different chemical species based on image analysis of backscattered electron SEM-images and energy-dispersive X-ray analysis dedicated to characterisation of straw ashes [35].

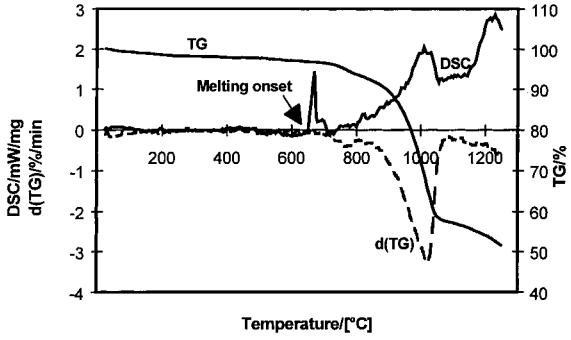

Fig. 6. STA curves for fly ash straw combustion.

Table 3
Selected CCSEM data (%,(w/w)) showing main constituents for the investigated ashes (modified from Refs. [34,35])

	KCl	K-/Ca-silicates [a]	Al-silicates	SiO_2
FA1	39.2	4.2	4.9	12.4
FA3	62.1	2.2	—	—
FA6	85.0	1.0	—	—
FA7	58.3	4.0	4.6	4.4
FA8	2.5	10.9	1.6	—
FA, coal	—	—	86.0	6.6
BA1	—	30.0	20.7	47.0
BA3	—	83.8	5.5	5.2
BA6	1.8	79.3	9.0	5.5
BA7	0.2	58.7	17.0	19.9
BA8	0.1	67.9	12.3	11.0
BA, coal	—	—	72.3	23.3

[a] K-, Ca-, and Si-rich amorphous particles.

STA curves for a typical fly ash (FA1) collected at the straw-fired boiler is shown in Fig. 6, where the increase in curve complexibility (compared to Fig. 3) is obvious. Referring to Fig. 6, the DSC curve is seen to show a distinct endothermic peak from 641° to 712°C, corresponding to an energy consumption of 176.1 J/g. As there is no simultaneous decrease in mass (TG curve), this peak corresponds to the onset of the melting of ash. With increasing temperatures, a general increase in the DSC signal is seen. On top of this general increase, two distinct peaks are seen, one ranging from ≈920° to 1050°C and another starting at ≈1150°C, which is not completely finished at 1250°C. The first of these two peaks is seen to occur simultaneously with a large decrease in mass, and since the

shape of the DSC peak and the d(TG) peak are quite – but not totally – alike, a large fraction – but not all – of the energy corresponding to this peak is used for evaporation of material rather than melting. As described earlier, the evaporation energies are estimated as the product of an estimated evaporation enthalpy and the d(TG) curve. In this case, the evaporation enthalpy of KCl has been used, since KCl constitutes a large part of this ash (∼40% (w/w), see Table 3) and is assumed to evaporate at these temperatures. For the last DSC peak, the simultaneous mass decrease is very low, and thus the energy corresponding to the area of this peak is predominantly used for melting of ash. The general increase of the DSC curve is caused by the fact that when great mass losses are occurring (as for this sample) the DSC baseline is shifted upwards [36]. This explanation is supported by the slope of the DSC curve, which is higher around the temperatures of rapid evaporation (800–1050°C) compared to temperatures <1100°C, where rapid evaporation ends, and the DSC baseline has found a new level at ≈1.5 mW/mg.

A typical set of STA curves for a silicate rich ash – e.g. the fly ash produced during coal combustion – is shown in Fig. 7. Nothing significant seems to occur until the temperature of 1180°C is reached, at which the DSC curve starts increasing. This is assumed to represent the melting onset. The DSC curve continuously increases until the termination of the experiment at 1390°C, at which point the DSC peak is not ended; that is to say the ash is not completely melted at 1390°C. Identification of specific chemical species melting in different temperature ranges between 1180° and 1390°C is not possible, but many alkali-rich alumina-silicates and other silica-rich phases typically melt in this temperature range [37]. However, the majority of the silica-rich phases in the ashes investigated are amorphous glasses and the DSC-peaks observed in this temperature range may also partly reflect an increase in heat capacity above the glass-transition temperature, an increase which amounts to 10–50% in silica-glasses [38]. Nevertheless, the peaks identify energy consumption linked to the physical change from solid glass to a liquid and the melting curve is thus calculated based on a comparison of areas. Energies used for the simultaneous evaporation are quantified by use of an evaporation enthalpy of 350 J/g, the uncertainty of which is compensated for by the fact that varying the evaporation enthalpy between 0.3 and 12 kJ/g does not affect the melting curves significantly [33]. The fraction of melt formed at 1390°C is determined by studying the sample structure (after cooling) in the SEM. The material which had not melted had maintained its original structure and occurred as discrete particles. The determination of the melt fraction being present at 1390°C was therefore made as an area evaluation of material of the original structure to that of the fused material.

In Figs. 8 and 9, the melting behaviours calculated on the basis of the STA curves are shown. Fig. 8 shows melting of fly ashes from straw combustion and Fig. 9 shows melting of bottom ashes from straw combustion and the two ashes from coal combustion. For the straw derived fly ashes (Fig. 8), the melting is seen to take place in two distinct temperature ranges: (1) between 630° and 750°C; and (2) >1000°C. The low-temperature range is believed to be caused by melting of an

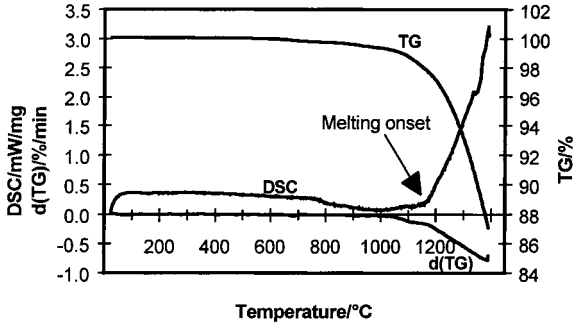

Fig. 7. STA curves for fly ash from coal combustion.

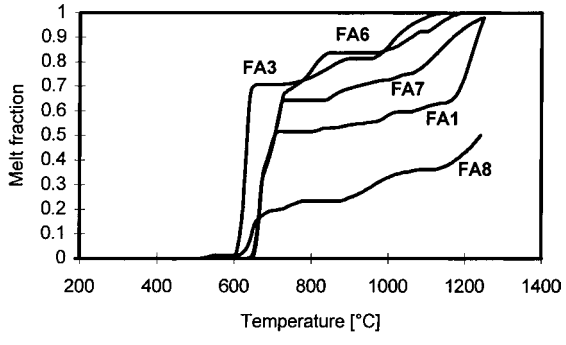

Fig. 8. Melting behaviour for fly ashes from straw combustion.

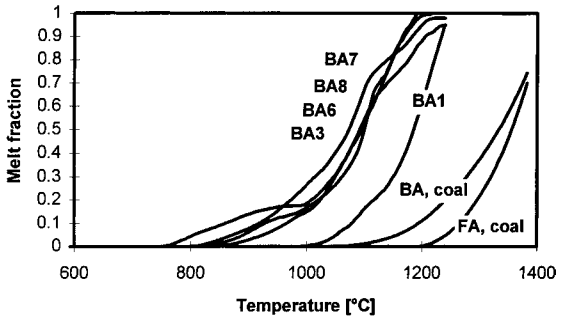

Fig. 9. Melting of bottom ashes from straw firing and ashes from coal firing.

eutectic mixture of potassium and calcium salts, while the high-temperature range is believed to include melting of the various silicates. The first melting peak for this fly ash is supposed to represent melting in a salt system containing large amounts of KCl and only minor quantities of 'other' K- and Ca-salts (chlorides and sulphates, the exact composition of which is not known), since the temperature agrees with the eutectic temperature for these systems and since these species have been found in the ash by means of CCSEM [34]. The melting curves for the bottom ashes from straw combustion and the coal-derived ashes show that melting starts at higher temperatures than for the fly ashes, which is consistent with the higher content of the relatively refractory silicates in these ashes.

In order to find a more systematic relation between ash chemistry and ash fusion, the CCSEM compositional data for the ashes is illustrated more clearly in a triangular diagram of (1) quartz and alumina silicates, (2) K- and Ca-silicates and (3) KCl (Fig. 10). The three end-members in the diagram were chosen to represent:

1. relatively refractory quartz and alumina silicates;
2. more easily fusible potassium and calcium dominated silicates; and
3. low-melting KCl [35,39].

The small numbers next to the 'data points' in the figure indicate the sum of the three end-members. For these data, the three end-members account for between 63 and 100% (w/w) of the composition of the samples (except for fly ash No. 8 which originates from combustion of straw of a contrasting composition). The compositional differences between the bottom and the fly ashes from straw combustion and the ashes from coal combustion are evident in this type of diagram, with the fly ashes from straw combustion being dominated by KCl and containing varying fractions of silicates, the bottom ashes from straw combustion being located on the 'silicate line', consisting almost exclusively of silicates, with varying ratios of 'quartz and alumino silicates' to 'K- and Ca-silicates', and with the coal-derived ashes consisting almost entirely of alumino silicates and quartz.

Comparing Figs. 8 and 10, it is seen that the fusion curves clearly reflect the compositional differences between the ashes: Fly ash Nos. 6 and 3, which contain the largest quantities of KCl, form larger quantities of

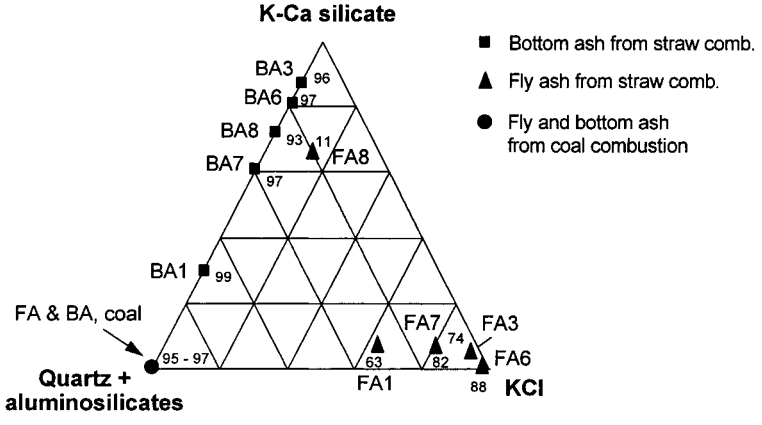

Fig. 10. CCSEM data presented in ternary diagram.

melt in the low-temperature range than the fly ash No. 7. Likewise, fly ash No. 7 shows larger melt fractions than fly ash No. 1, but higher melt fractions than the bottom ashes, which does not melt at all in the low-temperature range. Leaving fly ash No. 8 out of the discussion, a trend is thus seen for the fly ashes, of lower melt fractions for a given temperature, with an increase in silicate content relative to KCl content. This is in accordance with the low melting point of KCl compared to most silicates. This means that the melting behaviour of the ashes correlate with the position in the ternary diagram, i.e. moving (in composition) away from the KCl apex results in smaller melt fractions obtained in the low-temperature range.

Comparing Figs. 9 and 10, it is seen that for the four bottom ashes located closest to the 'K and Ca silicate' corner, the melting behaviours cannot really be distinguished, whereas they are all melting at temperatures lower than the bottom ash No. 1, which is located significantly closer to the 'quartz and aluminosilicate' corner. Likewise, the two ashes from coal combustion, consisting only of quartz and aluminosilicates melt at higher temperatures than the bottom ash No. 1 with the intermediate position on the silicate line. The general trend is, thus, that moving from the K- and Ca-silicate corner towards the quartz and aluminosilicate corner, the melting point of the ashes increases. This is in accordance with the more refractory nature of quartz and most aluminosilicates compared to K- and Ca-silicates, which may start melting at 740°C (the eutectic temperature in the K_2O–CaO–SiO_2 system).

It thus appears that the melting behaviours, as found by the STA, are in good agreement with the ash chemistry as determined by CCSEM and that the ternary diagram of dominant mineral categories (Fig. 10) can be used for a relative ranking of the melting behaviour of the ashes [33].

3.3. Repeatability of melting curves

Fig. 11 shows melting curves, respectively, for the fly ash from coal combustion (FA-coal), a fly ash from straw combustion (FA1) and a standard geological material (BSR-1) as obtained during repeating experiments. Starting with the straw-derived fly ash, it is seen from the curves that the repeatability of the onset of melting is very good – within 5°C, so is the slope of the first part of the curve. The first part of the curve

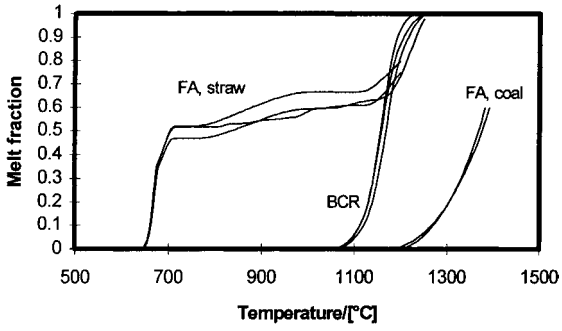

Fig. 11. Repeatability of melting curves.

corresponds to the very distinct peak occurring at low temperatures (641–712°C in Fig. 6), and since this peak is dependent on the salt chemistry of the sample, and this chemistry is quite simple (i.e. includes only a few possible reactions between the present species), the melting peak occurs at precisely the same temperature every time. The melt fraction obtained at these first peaks do deviate slightly, though; in this case, the level obtained is 50, 52 and 47% melt, respectively. This deviation is caused by both, the uncertainty of the method and the influence of sample inhomogeneity. For the rest of the melting curve, the uncertainty is somewhat larger, but still within 10% melt, which is judged to be acceptable. The larger uncertainty for the last part of the curve (>800°C) is due to the less distinct peaks corresponding to the melting of the silicate part of the ash. Since the peaks corresponding to silicate melting are less distinct, a precise characterization is dependent on a well-known baseline. For higher temperatures, drift in the DSC baseline cannot be avoided [36], which adds to the larger uncertainties. As stated above, the uncertainty is still within 10% melt, though. For the coal-derived fly ash, which consists mostly of silicates, the problem with less distinct peaks may generally lead to a larger uncertainty for the melting onset, but as can be seen, the repeatability is still quite good: onset of melting varies within 30°, and melt fractions at given temperatures are within 10% throughout the temperature interval from 650° to 1400°C.

To reduce uncertainties from sample inhomogeneity, repeatability was also tested by analyzing a well-characterized and homogenized geological standard material (a basalt, BCR1). Melting curves for these measurements are also shown in Fig. 11, and reveal

that onset is determined with a deviation of 15°C, melting completion temperature with a deviation of 5°C, and the melt fractions at given temperatures deviate at a maximum of 14% (melt). Based on these data, method repeatability is generally judged to be quite high.

4. Discussion

4.1. Correlation to standard ash-fusion test

For all fly and bottom ashes, the fusion was additionally characterized by the standard ash-fusion test, AFT (ISO540, 1981) [34]. This test implies heating of a cube of ash and determining the temperatures corresponding to:

1. rounding of the cube corners, at the initial deformation temperature, IDT;
2. the change in shape from cubic to hemispherical, at the hemispherical temperature, HT; and
3. flowing of the ash, at the fluid temperature, FT.

As an example of the agreement between results from the standard ash fusion test and those from the STA, the results of the standard AFT (DS/ISO540) are marked on the melting curve (for a straw ash) in Fig. 12. For this ash, it is seen that melting is detected by STA at temperatures as much as 105°C below the IDT, which is consistent with the previous criticism of the standard ash fusion tests [11–14]. The STA predicts significant melt formation (51%) to have occurred at the IDT. On the other hand, the melt fraction does not increase much for the next characteristic temperatures, since the hemispherical and the fluid temperature corresponds to a melt fractions, respectively, of 53 and 62% melt.

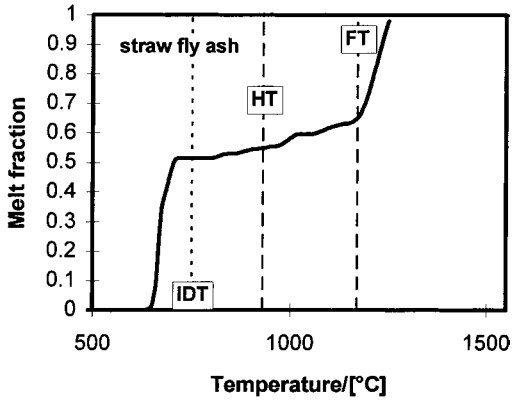

Fig. 12. Comparison of STA and standard AFT results.

Table 4
Relation between AFT temperatures and melt fractions determined by STA

	IDT			HT melt%	FT melt%
	T/°C	ΔT*	melt%		
FA1	750	−106	50.0	53.2	63.0
FA3	650	−50	70.1	70.6	71.9
FA6	710	−60	54.0	68.6	82.4
FA7	710	−63	54.0	65.0	73.2
FA8	790	−260	58.1	58.1	—
FA, coal	950	−35	2.5	53.4	—
BA1	910	79	0	52.7	—
BA3	870	−30	2.7	13.0	40.4
BA6	830	−60	7.0	55.8	—
BA7	900	−70	7.6	79.5	—
BA8	830	40	0	72.9	—
BA, coal	970	−158	11.0	—	—

$\Delta T^* = T_0 - \text{IDT}$.

For the rest of the presented ashes, the result of the comparison between the methods is given in Table 4. It is seen that, for the fly ashes, the melt formation starts at temperatures well below the IDT, ranging from 260°C below for the fly ash from Experiment 8 to 50°C below for the fly ash from Experiment 3. For the bottom ashes, melt formation is detected between zero and 95°C below the IDT, excepting the bottom ashes from experiments 1 and 8, for which melt is detected, respectively, 79° and 40°C above the IDT. For the fly ashes, substantial quantities of melt have been formed at the IDT, with an average of 49% melt found by the STA. However, the melt fractions detected for the bottom ashes at the IDT are much lower, on the average 3%. The reason for the STA to find no melt at the IDT for two silicate-rich bottom ashes might be that the rounding of the corners has been due to sintering of the ash instead of melting. At the hemispherical temperatures, melt fractions are generally between 35 and 70% melt, the bottom ashes generally showing smaller melt fractions than the fly ashes, whereas at the fluid temperature melt fractions measured, generally, were between 40 and 80%, the average being 73% melt. The AFT temperatures thus

seem to give a better description of the increasing melt fraction for the silicate-dominated ashes than for the salt-rich fly ashes from straw combustion. Overall, though, the standard AFT temperatures and the STA melting-behaviour curves seem to correlate qualitatively, as the three characteristic temperatures, typically, are all located in the temperature range corresponding to 3–80% melt in the ash. A further and more detailed comparison between the standard AFT and the STA melting behaviour results is presented elsewhere [33].

These findings generally support previous criticism [11–14] on the ground that the IDT does not indicate the melting onset. The IDT has been known to indicate the temperature, at which ash particles in an operating furnace have cooled sufficiently to have only a slight tendency to stick together [40], but with melt fractions of 30–60%, the stickiness of the ash may be somewhat higher than only 'slight', meaning that keeping furnace exit gas temperatures below the IDT (as found by conventional AFT) does not guarantee avoidance of deposit problems in the boiler convective pass.

4.2. Method limitations

At present, the described STA method works as an expert tool. The STA measurements are easy and simple to perform, the repeatability of the results is good, and the measurement procedure can easily be standardized. The interpretation of the STA signal, that is the conversion from the STA curves to the melting curve is, on the other hand, not simple and cannot at the moment be standardized. Interpretation requires detailed knowledge of the chemical species in each ash sample (as provided by CCSEM or XRD analysis) and the chemical reactions occurring between these. This is necessary for expressing the melt fraction as a mass percent, but is also important to avoid energies, related to solid-phase transitions occurring simultaneously to melting, from being wrongly detected as such.

4.3. Applicability of the results

Compared to conventional methods, the new method provides an improved and more detailed characterization of the melting process occurring in ashes during heating. The results reveal the temperature at which the first melt is formed in the ash, and therefore gives important information to boiler designers. Furthermore, the melting curves can be used as input to mechanistic modelling of ash deposit formation by inertial impaction, which will hopefully improve the understanding of ash-deposit formation mechanisms during biomass and/or coal combustion.

5. Conclusions

A new experimental method for quantification of ash melting has been developed. Using the new method, a conventional STA apparatus is employed, and the melting is detected as endothermic reactions involving no change in mass. The DSC signal is transferred into a melting curve (showing the melt fraction in the ash as a function of temperature) either by a simple comparison of the areas below the melting curve or by accounting for the relevant melting enthalpies. The execution of the measurement is simple and the repeatability of the results is very good. The subsequent conversion of the STA curves to a melting curve requires knowledge of the identity of chemical species in the ash – as provided by CCSEM analysis, for instance – and the involved chemistry.

The method has so far been tested on a number of simple salt mixtures, for which the measured melting behaviour agrees with the predictions from phase diagrams, and a number of ashes collected during combustion of straw, co-combustion of straw and coal, and coal combustion, for which melt was typically detected between 40° and 110°C below the corresponding melting onset temperature found by the standard AFT. Characterizing the fusion by STA provides a continuous description of the ash melting as compared to the discrete description obtained by conventional methods, and a precise determination of the onset of ash fusion. As ash melting has a major impact on the deposit formation tendency, the presented detailed ash fusion determination improves the prediction of ash deposition propensities. Since the measurement principle is not especially designed for studying ashes from combustion, the method could as well be used for characterizing melting of other kinds of materials, for which a detailed knowledge about the melting behaviour could be useful.

Acknowledgements

This work was carried out as part of the *C*ombustion and *H*armful *E*mission *C*ontrol (CHEC) research programme at the Department of Chemical Engineering, Technical University of Denmark. The CHEC research program is cofunded by ELSAM (The Jutland–Funen Electricity Consortium), ELKRAFT (The Zealand Electricity Consortium), the Danish Technical Research Council, the Danish and the Nordic Energy Research programmes.Mrs. Gurli Mogensen (from Haldor Topsoe A/S) is acknowledged for her invaluable contributions to the interpretation of the DSC curve behaviour during the long and troublesome running-in of the apparatus.

References

[1] S.A. Benson, M.L. Jones, J.N. Harb, in L.D. Smoot (Ed.), Fundamentals of Coal Combustion for Clean and Efficient Use, Elsevier, New York, 1993, pp. 299.
[2] R.W. Bryers, Prog. Energy Com. Sci. 22 (1996) 29.
[3] S. Srinivasachar, J.J. Helble, C.B. Katz, A.A. Boni, in R.W. Bryers, K. Vorres (Eds.), Engineering Foundation Conference on Mineral Matter and Ash Deposition from Coal. Engineering Foundation, New York, 1990, pp. 111.
[4] P.M. Walsh, A.N. Sayre, D.O. Loehden, L.S. Monroe, J.M. Beér, A.F. Sarofim, Prog. Energy Comb. Sci. 16 (1990) 327.
[5] G.H. Richards, P.N. Slater, J.N. Harb, Energy and Fuels 7 (1993) 774.
[6] B.J. Skrifvars, R. Backman, M. Hupa, preprint of papers presented at the 211th ACS National Meeting, New Orleans, LA, March 24–28, Vol. 41, No. 2, American Chemical Society, 1996, pp. 640.
[7] ISO 540, International Standard Organisation, 1981.
[8] DIN 51730, German Standard, 1984.
[9] ASTM D1857-87, American Society for Testing and Materials, 1987.
[10] AS1038.15, Australian Standards Association, 1987.
[11] C.D.A. Coin, H. Kahraman, A.P. Peifenstein, in L.L. Baxter, R. DeSollar (Eds.), Engineering Foundation Conference on Application of Advanced Technology to Ash-Related Problems, Plenum Press, Plenum Press, New York and London, 1996, p. 187.
[12] G.P. Huffman, F.E. Huggins, G.R. Dunmyre, Fuel 60 (1981) 585.
[13] F.E. Huggins, A.K. Deborah, G.P. Huffman, Fuel 60 (1981) 577.
[14] T.F. Wall, R.A. Creelman, R.P. Gupta, S. Gupta, C. Coin, A. Lowe, in L.L. Baxter, R. DeSollar (Eds.), Engineering Foundation Conference on Application of Advanced Technology to Ash-Related Problems, Plenum Press, New York and London, 1996, p. 541.
[15] E.J. Raask, J. Thermal Anal. 16 (1979) 91.
[16] A. Sanyal, I.W. Cumming, in R.W. Bryers (Ed.), US Engineering Foundation Conference on Fouling and Slagging Resulting from Impurities in Combustion Gases, Engineering Foundation, New York, 1981, p. 329.
[17] J.R. Gibson, W.R. Livingston, in S.A. Benson (Ed.), Engineering Foundation Conference on Inorganic Transformations and Ash Deposition during Combustion, ASME, New York, 1992, pp. 425.
[18] A. Sanyal, A.K. Mehta, in J. Williamson, F. Wigley (Eds.), Engineering Foundation Conference on Impact of Ash Deposition on Coal Fired Plants, Taylor and Francis, Washington, 1994, pp. 445.
[19] I.W. Cumming, A. Sanyal, in R.W. Bryers (Ed.), US Engineering Foundation Conference on Fouling and Slagging Resulting from Impurities in Combustion Gases, Engineering Foundation, New York, 1981, p. 135.
[20] R.E. Conn, L.G. Austin, Fuel 63 (1984) 1664.
[21] I.W. Cumming, W.I. Joyce, J.H. Kyle, in R.E. Barrett (Ed.), Engineering Foundation Conference on Slagging and Fouling Due to Impurities in Combustion Gases, Engineering Foundation, New York, 1985, p. 555.
[22] T.F. Wall, R.P. Gupta, P. Polychroniadis, G.C. Ellis, R.C. Ledger, E.R. Lindner, The Strength, Sintering, Electrical Conductance and Chemical Character of Coal Ash Deposits, NERDDC Project No. 1181 – Final Report, Vol. 1, Summary Report, 1989.
[23] E.C. Winegartner, B.T. Rhodes, J. Eng. Power 97 (1975) 395.
[24] K.W. Vorres, J. Eng. Power 101 (1979) 497.
[25] V.R. Gray, Fuel 66 (1987) 1230.
[26] W.G. Lloyd, J.T. Riley, M.A. Risen, S.R. Gilleland, R.L. Tibbits, Energy and Fuels 4 (1989) 325.
[27] S.V. Vassilev, K. Kitano, S. Takeda, T. Tsurue, Fuel Process. Techn. 45 (1995) 27.
[28] R. Backman, Sodium and Sulfur Chemistry in Combustion Gases, Academic Dissertation, Åbo Academy University, Åbo, Finland, 1989.
[29] K.E. Eriksen, Report on Ash Fusion Determination for Straw Ash, Internal Report, Studstrupvaerket, Aarhus, Denmark, 1989 (in Danish).
[30] S. Westborg, Round Robin Test – Analysis of Straw and Straw Ash. Internal report, Biomass Ash Characterisation Project, dk-TEKNIK, Soeborg, Denmark, 1995 (in Danish).
[31] R. Backman, M. Hupa, E. Uppstu, Tappi J. 70(6) (1987) 123.
[32] E.M. Levin, C.R. Robbins, H.F. McMurdie, H.F., Phase Diagrams for Ceramists, vol. 1, The American Ceramic Society, Columbus, OH, 1964.
[33] L.A. Hansen, Melting and sintering of ashes, Ph.D. Thesis, Department of Chemical Engineering, Technical University of Denmark, 1998, ISBN....
[34] F.J. Frandsen, L.A. Hansen, H.S. Sørensen, and K. Hjuler, Characterisation of ashes from biofuels, Final Report from EFP-95 Project, Journal No. 1323/95-0007, The Danish Energy Research Programme, 1998, ISBN 87-7782-000-2.
[35] H.S. Sørensen, in L.L. Baxter, T.F. Wall, R.P. Gupta (Eds.), Engineering Foundation Conference on Impact of Mineral

Impurities in Solid Fuel Combustion, Plenum Press, New York and London, 1997, in print.
[36] Netzsch, personal communication, 1995.
[37] E. Raask, Mineral Impurities in Coal Combustion, Hemisphere Publishing Corporation, Springer-Verlag, New York, 1985.
[38] P. Richet, Y. Bottinga, Rev. Geophy. Space Phy. (1986) 1.
[39] L.A. Hansen, F.J. Frandsen, H.S. Sørensen, P. Rosenberg, K. Hjuler, K. Dam-Johansen, in L.L. Baxter, T.F. Wall, R.P. Gupta (Eds.), Engineering Foundation Conference on Impact of Mineral Impurities in Solid Fuel Combustion, Plenum Press, New York and London, 1997, in print.
[40] T.R. Bott, in S.A. Benson (Ed.), Engineering Foundation Conference on Inorganic Transformations and Ash Deposition During Combustion, ASME, New York, 1992, pp. 191.